



# Early-Age Cuprizone Exposure Induces Region-Specific Demyelination and Neuroinflammation in Mice

May Rokach<sup>1</sup> · Gilad Levy<sup>1</sup> · Galit Elad-Sfadia<sup>2</sup> · Boaz Barak<sup>1,2,3</sup>

Received: 19 December 2025 / Accepted: 2 February 2026  
© The Author(s) 2026

## Abstract

Myelin, essential for rapid nerve conduction and axonal integrity in the central and peripheral nervous systems, is compromised in demyelinating diseases, leading to neurological deficits and progressive neurodegeneration. Although remyelination can occur, regeneration in adults is often limited, resulting in incomplete repair and impaired nerve function. In multiple sclerosis (MS), an immune-mediated demyelinating disease with diverse clinical phenotypes, progression and disability correlate with demyelination and failed remyelination, influenced by genetic and environmental factors. A well-established method to study MS-like demyelination and its cellular and molecular mechanisms utilizes cuprizone (CPZ), extensively studied in adult rodents. Although early-onset demyelination often causes lifelong disability, its pathophysiology remains poorly understood, underscoring the need for models to dissect its biological features. Here, we characterized the effects of early-age CPZ-induced demyelination in juvenile naïve mice, focusing on region-specific vulnerability and neuroinflammatory responses. One-month-old mice were exposed to 0.2% CPZ for five weeks, followed by behavioral, cellular, and transcriptomic analyses. Susceptibility to the early-exposure of CPZ varied between the analysed brain regions. The midline corpus callosum and motor cortex were highly vulnerable, showing marked reductions in myelin together with elevated microglial activation. Other regions, including the hippocampus and amygdala, showed milder susceptibility, often restricted to changes in *Mbp* or *Ibal* transcript levels without corresponding alterations in oligodendrocyte or microglial cell numbers. Behaviorally, early CPZ exposure reduced locomotor activity but did not produce robust anxiety-like or cognitive deficits. Together, these findings reveal distinct regional patterns of early-onset demyelination and neuroinflammation and support CPZ exposure in juvenile mice as a relevant model for multifocal juvenile demyelination, including paediatric-onset MS, and its impact on neurodevelopment.

**Keywords** Myelin · Multiple sclerosis · Oligodendrocytes · Microglia · Early onset demyelination · Remyelination · Cuprizone

## Introduction

Myelin, a lipid-rich sheath encasing axons in the central and peripheral nervous systems (CNS and PNS), enables saltatory conduction (Frankenhaeuser, 1952), enhances signal transmission (Seidl, 2014), and maintains axonal integrity (Saab et al., 2013). Variations in myelin structure support neural plasticity (Nave & Werner, 2014), whereas damage (Touma & Muccilli, 2022) or abnormalities (Rokach et al., 2024) result in neurological deficits. Demyelination, the process of myelin loss and degradation, leads to functional impairment and progressive neurodegeneration (Franklin & Kotter, 2008). Although remyelination occurs, it is often incomplete (Franklin & Ffrench-Constant, 2008) in adults due to reduced regenerative capacity (de Faria et al., 2021),

✉ Boaz Barak  
boazba@tauex.tau.ac.il

<sup>1</sup> Sagol School of Neuroscience, Tel-Aviv University, Tel-Aviv, Israel

<sup>2</sup> Faculty of Social Sciences, School of Psychological Sciences, Tel-Aviv University, Tel-Aviv, Israel

<sup>3</sup> Faculty of Life Sciences, School of Neurobiology, Biochemistry & Biophysics, Tel-Aviv University, Tel-Aviv, Israel

resulting in thinner myelin sheaths and impaired nerve function (Franklin, 2002).

In the CNS, oligodendrocytes (OLs) form myelin by extending their plasma membranes around axons (Nave & Werner, 2014). OLs develop from OL precursor cells (OPCs), which migrate, proliferate, and differentiate into mature myelinating OLs (mOLs) (Bradl & Lassmann, 2010). OPCs make up 5–8% of cells in the adult human brain (Chang et al., 2000). They maintain lifelong myelination by responding to neural activity (Noori et al., 2020), promoting learning-dependent myelin changes (Xin & Chan, 2020), and enabling repair after injury (Franklin & Ffrench-Constant, 2008). Microglia, the resident immune cells of the CNS, also support myelination by secreting factors that drive OPC migration, proliferation (Santos & Douglas Fields, 2021), and differentiation (Bar & Barak, 2019). During demyelination, microglia clear myelin debris (Lampron et al., 2015), facilitating OL access to lesion sites (Domingues et al., 2016) and promoting remyelination (Lloyd & Miron, 2019) (Fig. 1).

Multiple sclerosis (MS), an inflammatory CNS disease, is characterized by immune-mediated myelin damage (Dighriri et al., 2023; Murúa et al., 2021). MS lesions, visualized by magnetic resonance imaging (MRI) (Filippi et al.,

2019), may occur with or without clinical symptoms (Siva, 2013) and are unevenly distributed across the CNS (Calabrese et al., 2010; Eden et al., 2019). The phenotype and severity of symptoms depend on lesion location (Kincses et al., 2011; van Munster et al., 2015), while disease progression and disability are strongly linked to failed remyelination (Franklin, 2002; Lubetzki et al., 2020). Although multiple genetic (Patsopoulos, 2018) and environmental (Ascherio, 2013) risk factors have been identified, MS has no single etiology (Dobson & Giovannoni, 2019).

Globally, MS affects ~35.9 per 100,000 individuals (Walton et al., 2020), with a 2:1 female-to-male ratio. Most cases are adult-onset MS (AOMS), with onset between ages 20 and 40 (Dighriri et al., 2023). Diagnosis usually occurs 1–3 years after symptom onset (Jakimovski et al., 2023; Patti et al., 2022), though demyelination may precede diagnosis by years or decades (Jakimovski et al., 2023; Patti et al., 2022; Van Der Valk & Amor, 2009). Paediatric-onset MS (POMS), representing up to 10% of cases, is diagnosed before age 18 (Capasso et al., 2023). Unlike AOMS, POMS presents with a 1:1 gender ratio before puberty and often manifests as multifocal rather than focal symptoms (Fisher et al., 2020). POMS is associated with high inflammation at onset, greater risk of early disability, and accelerated

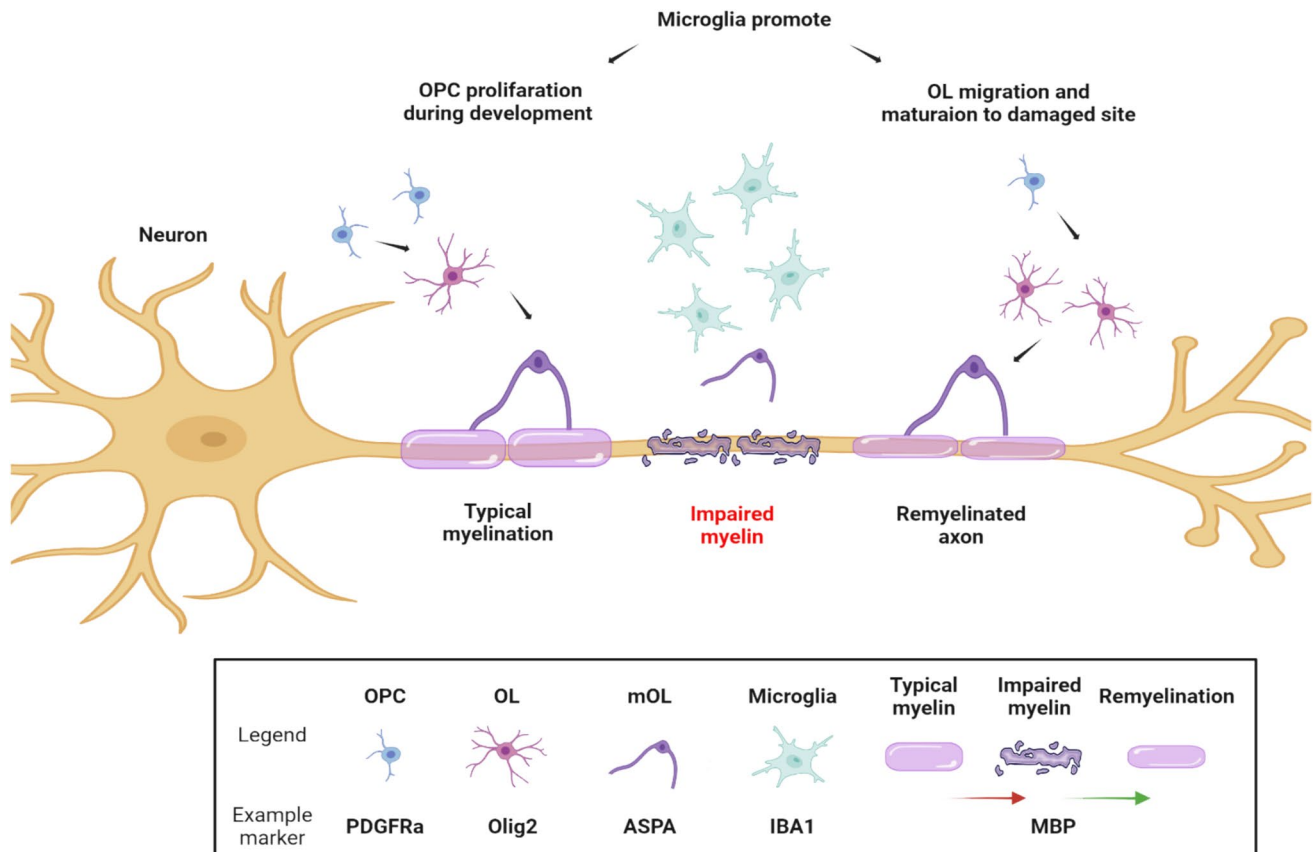


**Fig. 1** OL-microglia interactions in myelin development, damage and recovery. Platelet-derived growth factor receptor alpha (PDGFR $\alpha$ ), aspartoacylase (ASPA), Ionized calcium-binding adapter molecule 1 (Iba1), myelin basic protein (MBP).

cognitive decline (Ruet, 2018), with disability milestones reached at younger ages than in AOMS (McKay et al., 2019).

Cuprizone (CPZ), a copper-chelating toxin administered through chow (Hochstrasser et al., 2017), is a widely used rodent model of demyelination. CPZ exposure produces well-characterized lesions (Kipp et al., 2009; Torkildsen et al., 2008; Vega-Riquer et al., 2019; Zhan et al., 2020), with reduced myelin proteins expression and increased microglial activation (Praet et al., 2014; Zendedel et al., 2013)—features that parallel MS pathology (Ponath et al., 2018; Tepavčević & Lubetzki, 2022; Voet et al., 2019). CPZ is favored because lesions are reversible after diet cessation (Matsushima & Morell, 2001; Vega-Riquer et al., 2019; Zhan et al., 2020). While its exact mechanism is not fully

understood (Zirngibl et al., 2022), CPZ likely induces mOL apoptosis (Bénardais et al., 2013), triggering glial activation, myelin debris clearance (Lampron et al., 2015; Skripuletz et al., 2013) and expose axons (Zhan et al., 2020). Traditionally, CPZ has been introduced in adult mice (6–8 weeks, approximating ~25 years in humans (Flurkey et al., 2007)), to study adult-onset demyelination (Fig. 2A). However, investigating early-onset demyelination is crucial, as juvenile demyelination is associated with lasting disability.

Previous studies in juvenile animals have characterized behavioral (Wang et al., 2013) and molecular (Pfeifenbring et al., 2015) effects of CPZ, focusing mainly on the corpus callosum (CC) and motor cortex—regions validated in adult CPZ models. Yet, because POMS is a multifocal disease and CPZ acts systemically, it is essential to examine the relative

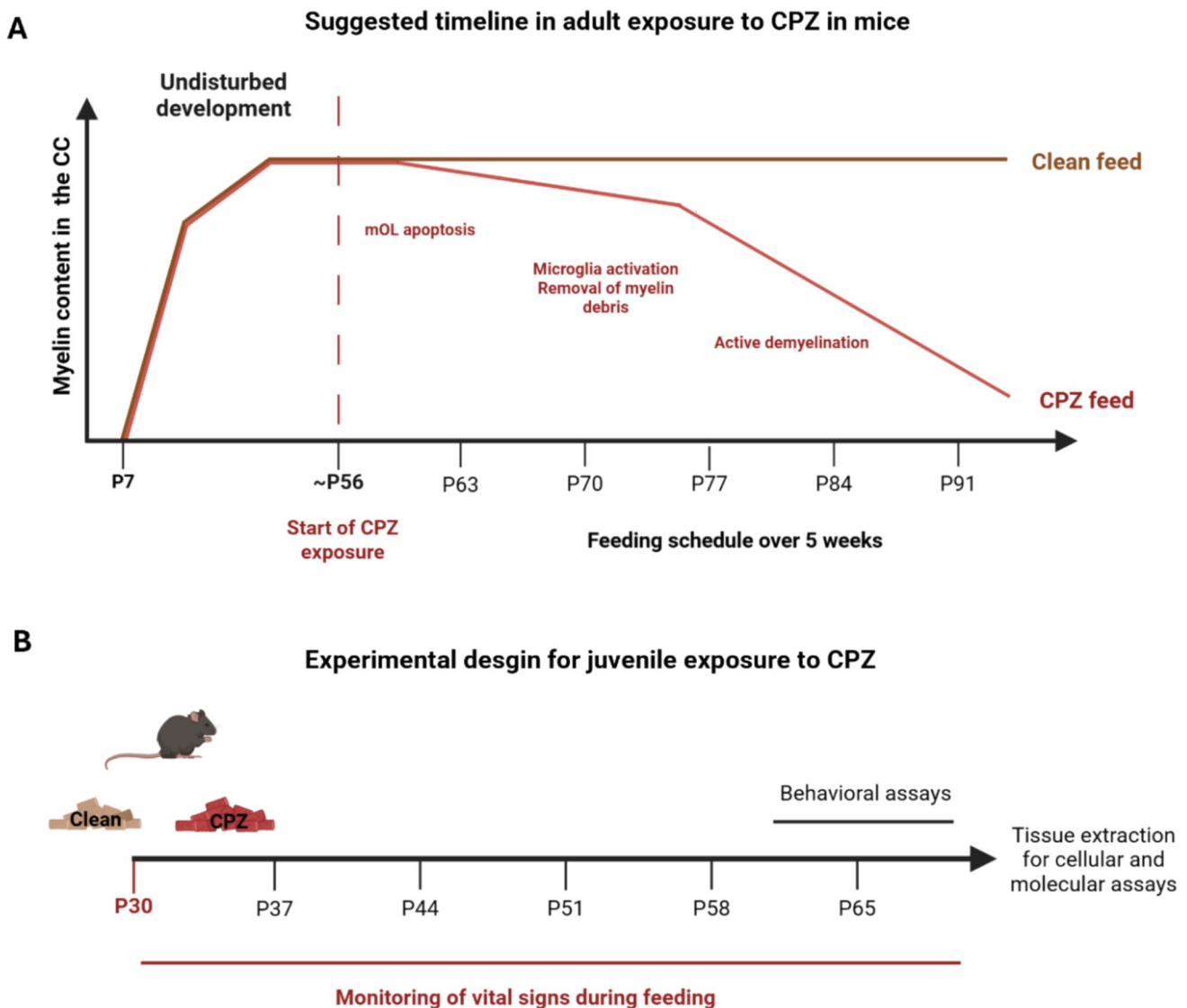


**Fig. 2** CPZ experimental design and cellular changes. **(A)** Suggested timeline of cellular and myelin content changes during CPZ exposure in mice, based on previous work (Bénardais et al., 2013; Lampron et

al., 2015; Skripuletz et al., 2013; Zhan et al., 2020; Zirngibl et al., 2022). **(B)** The experimental design used in this study

susceptibility of additional brain regions and the interplay between neuroinflammation and mOL loss.

Here, we investigated early-age demyelination by exposing one-month-old mice to 0.2% CPZ in chow for five weeks (Fig. 2B). Behavioral, anatomical, cellular, and transcriptomic analyses revealed distinct regional susceptibilities to CPZ-induced demyelination and neuroinflammation. Our findings underscore the importance of regional vulnerability and support the CPZ model as a tool for studying early-onset demyelination, with direct relevance for POMS research.

## Results

### Gross Anatomical Changes in Early Exposure to Cuprizone

Because CPZ is a toxin administered systemically, the physical condition of experimental mice was carefully monitored throughout the study. Both control and CPZ-exposed groups exhibited steady weight gain over time; however, the CPZ-treated mice maintained a significantly lower overall body weight compared with clean-diet controls (Fig. 3A). Brain weights did not differ significantly between groups (Fig. 3B), and no other overt physical or clinical symptoms were observed in either group (data not shown).

To assess the anatomical impact of early-onset demyelination, we measured the total area of the lateral ventricles (Bermel & Bakshi, 2006; Millward, 2020). No significant differences were detected between groups (Fig. 3C). In contrast, consistent with CPZ's known effects, the midline CC

(mCC)—particularly at the level of the anterior commissure (bregma 0.48) (Zhan et al., 2020)—was significantly reduced in area in CPZ-exposed mice (Fig. 3D), confirming the mCC's high vulnerability to demyelination.

### Brain Regions of Interest Chosen for Analysis

Regions of interest (ROIs) were chosen based on three criteria: (i) brain regions implicated in prior studies of MS patients, (ii) brain regions previously validated in adult CPZ exposure studies, and (iii) heavily myelinated brain regions with functional relevance for demyelination analysis. A graphical overview and a summary of the supporting studies are presented in Table 1. Relevant abbreviations: midline corpus callosum (mCC), cortex (CTX), striatum (STR), hippocampus (Hipp), amygdala (Amyg), hypothalamus (Hypo).

### Region-Specific Susceptibility to Demyelination

To assess demyelination, we performed immunofluorescence (IF) staining for myelin basic protein (Mbp; Fig. 4A) and measured *Mbp* transcript levels using qPCR (Fig. 4B). Because of variability in the mCC across animals, and its reduction in size following CPZ exposure, IF results for the mCC are presented as the mean Mbp intensity within the region (Fig. 4C). For all other ROIs, Mbp levels were quantified within a fixed-size box (Fig. 4D). While a significant reduction in *Mbp* transcript levels was observed across all ROIs in the CPZ group compared to Clean, Mbp protein intensity was significantly lower only in specific regions, namely the mCC, CTX, and Hipp. In contrast, Mbp intensity

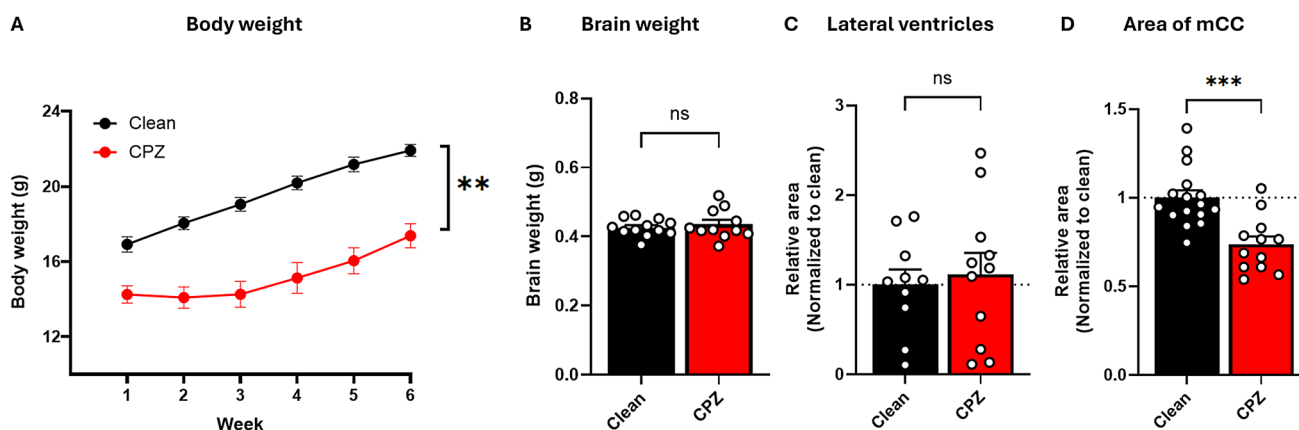


**Fig. 3** Gross anatomical changes in early exposure to CPZ. **(A)** Body weight was significantly lower in CPZ-exposed mice compared with Clean group over time (Clean,  $n=12$ ; CPZ,  $n=13$ ; two-way ANOVA: time factor,  $P<0.001$ ; treatment factor,  $P<0.001$ ; interaction,  $P=0.0046$ ). B-C unchanged neuroanatomical properties between

groups **(B)** Brain weight (Clean,  $n=12$ ; CPZ,  $n=11$ ; Student's  $t$ -test,  $P=0.519$ ). **(C)** Area of lateral ventricles (Clean,  $n=10$ ; CPZ,  $n=11$ ; Student's  $t$ -test,  $P=0.699$ ). **(D)** Area of mCC was significantly lower in CPZ exposure group compared to Clean group (Clean,  $n=16$ ; CPZ,  $n=12$ ; Student's  $t$ -test,  $P=0.0002$ ).

**Table 1** Regions of interest chosen for analysis

	Functionality and relevance to MS	Relevance in the CPZ model
Corpus callosum (mCC)	Heavily myelinated (Degraeve et al., 2022) and periventricular areas (Tonietto et al., 2023) are particularly susceptible to demyelination lesions	The mCC is particularly vulnerable to demyelination and serves as a key region for assessing demyelination (Zhan et al., 2020)
Cortex (CTX)	Motor dysfunction is among the most prevalent symptoms of MS (Younger, 2023) and is utilized to evaluate the disability score in MS patients (Kurtzke Expanded Disability Status Scale - Multiple Sclerosis Centers of Excellence, 2026)	The CTX of the mouse serves as a prominent example of grey matter demyelination (Lubrich et al., 2022; Zhan et al., 2020)
Striatum (STR)	Periventricular regions generally exhibit a higher lesion load (Tonietto et al., 2023), and striatal damage is correlated with motor disability in long-term patients (Cavallari et al., 2014; Kerbrat et al., 2020)	The susceptibility of striatal glial cells to CPZ has been investigated previously (Goldberg et al., 2015). In the present study, we focused on the dorsomedial striatum, which best represents a periventricular area
Hippocampus (Hipp)	Damage to the Hipp in MS is a significant contributor to the cognitive deficits associated with the disease (Rocca et al., 2018)	Previous studies have indicated that CPZ exposure leads to demyelination and axonal loss in the Hipp (Hoffmann et al., 2008)
Amygdala (Amyg)	Crucial for learning and goal directed behaviors (Averbeck & Murray, 2020) but its susceptibility to MS lesions remains less well defined, although it may partially account for the high prevalence of depression and anxiety in patients (Peres et al., 2022)	In CPZ models, mice show reduced learned fear conditioning, suggesting functional involvement of amygdalar circuits (Kopanitsa et al., 2021)
Hypothalamus (Hypo)	The Hypo plays a vital role in cognitive and autonomic functions (Averbeck & Murray, 2020; Burdakov & Peleg-Raibstein, 2020; Caria, 2023) and is known to be affected in MS (Anagnostouli et al., 2020; Genç et al., 2023)	Limited information is available regarding Hypo susceptibility to CPZ (Dorikhani et al., 2024; Sen et al., 2020)

remained unchanged in the STR, Amyg, and Hypo. Because CPZ is known to induce apoptosis in mOLs (Bénardais et al., 2013), we also evaluated OL populations in the same ROIs by quantifying ASPA-positive mOLs (Fig. 4E, F) and PDGFR $\alpha$ -positive OPCs (Fig. 4G, H). The number of mOLs increased in the Hypo of CPZ-exposed mice compared to Clean group and remained unchanged in all other ROIs. The number of OPCs did not differ between groups in any of the analyzed ROIs. The high number of PDGFR $\alpha$ -positive cells in the CTX, compared with other brain regions, is consistent with previous work (Erö et al., 2018; Oligodendrocyte heterogeneity in the mouse juvenile & adult central nervous system | Science, 2016; Valério-Gomes et al., 2018; Zheng et al., 2018).

## Region-Specific Susceptibility to Neuroinflammation

As previously described, neuroinflammation is a key component of pathology in both MS and the CPZ model of demyelination (Luo et al., 2017; Pott et al., 2009; Skripuletz et al., 2013; Voet et al., 2019). To assess microglial activation, we quantified Iba1-positive cells, a marker of activated microglia (Ito et al., 1998). For the mCC, cell counts were normalized to the mCC area (Fig. 5A), whereas in all other ROIs, absolute counts were obtained within a fixed-size box (Fig. 5B). Here, we observed a significant increase in Iba1-positive cells in the mCC of the CPZ group compared to the Clean group, while no significant differences were detected in the other brain regions analyzed.

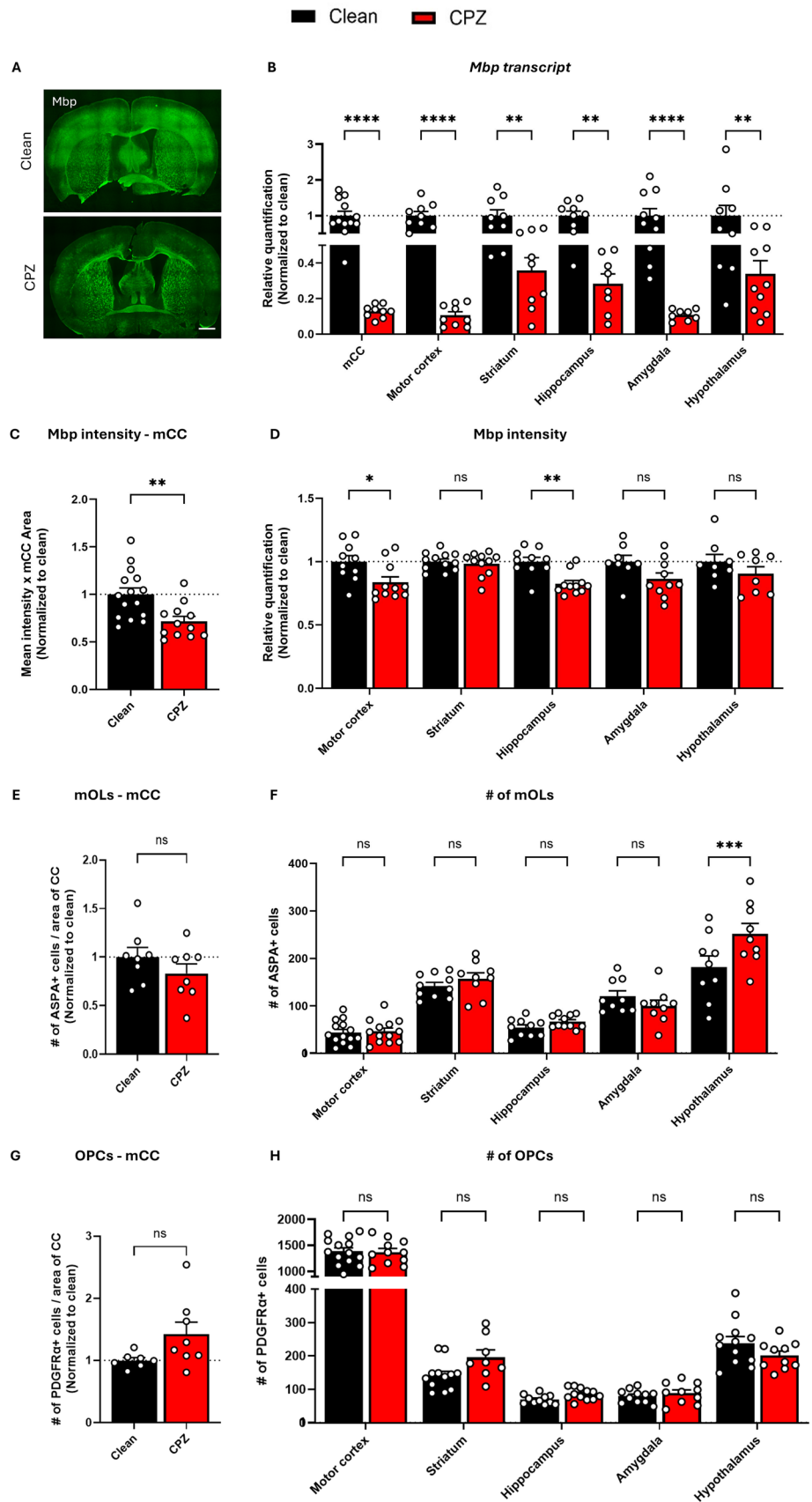
In addition, tissue from the same ROIs at corresponding bregma levels was collected for qPCR analysis of *Iba1* transcript expression (Fig. 5C). A significant increase in *Iba1* transcript level was observed in the mCC, STR, Amyg, and Hypo, but no significant change was observed in the CTX or Hipp.

## Behavioral Outcomes of Early-Age Demyelination

Alongside cellular and molecular parallels between demyelination in human disorders and CPZ-exposed mice, prior work has shown that CPZ treatment also induces behavioral abnormalities resembling myelin-related neurological symptoms (Kopanitsa et al., 2021; Sen et al., 2019, 2020). To evaluate the behavioral consequences of early-onset demyelination, we employed four behavioral assays known to be sensitive to CPZ exposure: the open field test (anxiety and locomotor activity), the elevated zero maze (EZM; anxiety), the rotarod test (motor coordination), and the novel object recognition test (short-term memory and cognition). Each of these behaviors is linked to the functional role of one or more of the previously analyzed ROIs.

Early CPZ exposure did not significantly alter anxiety-like behavior in the open field test (Fig. 6A). However, locomotor activity, quantified as the total distance traveled over 60 min, was significantly reduced in CPZ-treated mice compared to clean-diet controls (Fig. 6B). The EZM test likewise did not reveal any significant changes in anxiety-like behavior (Fig. 6C), and motor performance on the rotarod test remained unchanged between groups (Fig. 6D).

**Fig. 4** Region-specific susceptibility to demyelination in early age. **(A)** Representative IF images of Mbp staining **(B)** *Mbp* transcript levels measured by qPCR (Clean, n=9-12; CPZ, n=8-11); **(C, D)** Quantification of Mbp intensity in IF images (Clean, n=8-15; CPZ, n=8-12). **(E, F)** Number of mOLs (Clean, n=9-14; CPZ, n=8-13); **(G, H)** Number of OPCs (Clean, n=7-14; CPZ, n=8-12); Statistical significance was assessed by two-way ANOVA: ns= nonsignificant, \* $p < .05$ , \*\* $p < .01$ , \*\*\* $p < .001$ , \*\*\*\* $p < .0001$ . Scale bar: 100 $\mu$ m.



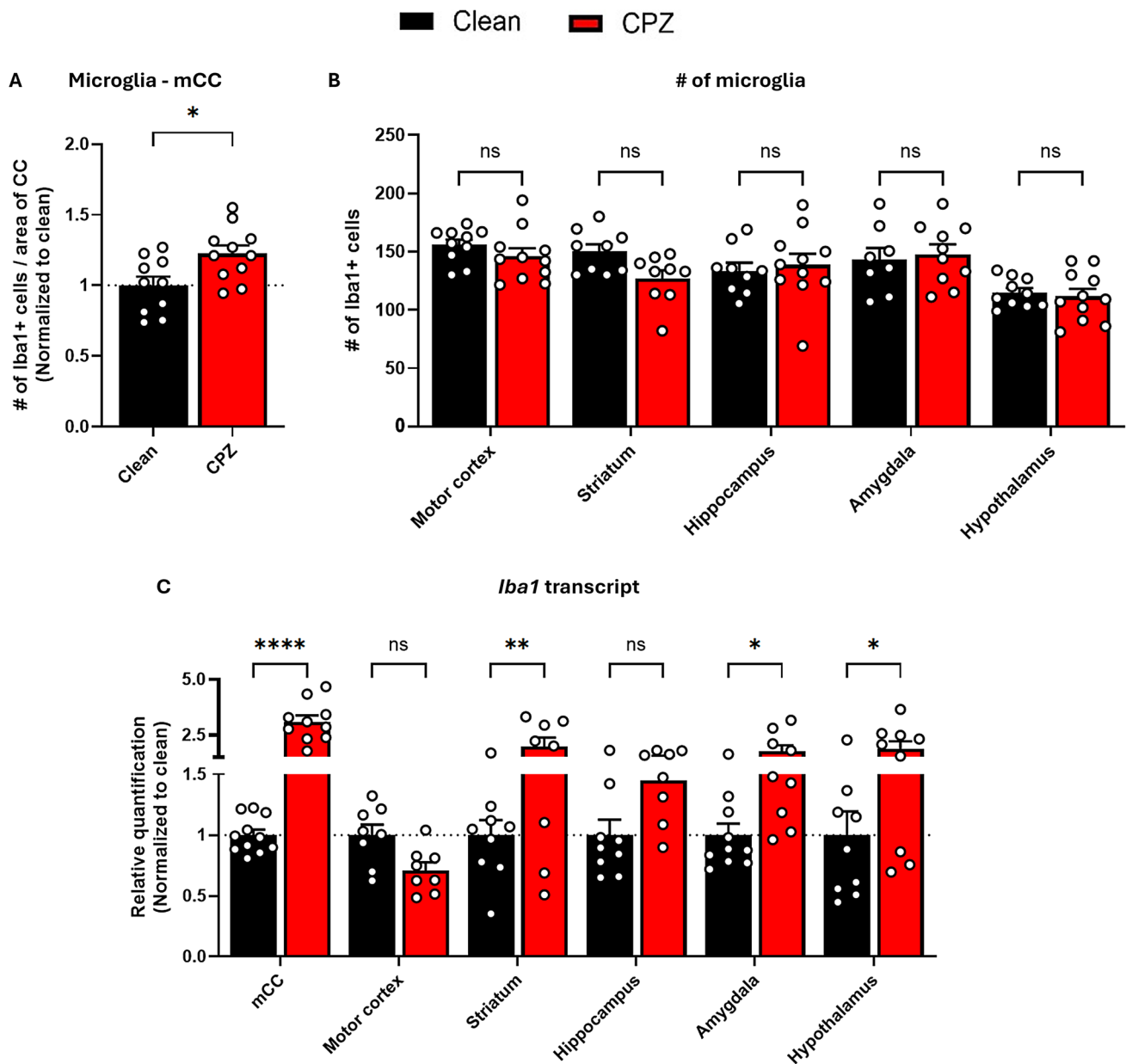


**Fig. 5** Region-specific susceptibility to neuroinflammation in early age. **(A, B)** Quantification of Iba1 positive cells in IF images (Clean, n=8-11; CPZ, n=8-10). **(C)** *Iba1* transcript levels measured by

qPCR (Clean, n=8-11; CPZ, n=8-11).; Statistical significance was assessed by two-way ANOVA: ns=nonsignificant, \*p<.05, \*\*p<.01, \*\*\*\*p<.0001.

Cognitive performance in the novel object recognition test showed no group differences: both CPZ-exposed and clean-diet controls were able to discriminate between familiar and novel objects (Fig. 6E), and recognition indices did not differ significantly between groups (Fig. 6F).

## Discussion

Myelin, OLs, and microglial activation are central to demyelination and remyelination processes in the CNS (Bar & Barak, 2019; Franklin & Kotter, 2008; Hamilton & Rome, 1994; Nave & Werner, 2014; Santos & Douglas Fields, 2021; Xin & Chan, 2020). Disruption of their interaction often results in scar formation and progressive neurological disability. Demyelination has been widely studied in adult models, where myelin volume is stable and OL turnover is low (de Faria, et al., 2021). These studies largely address

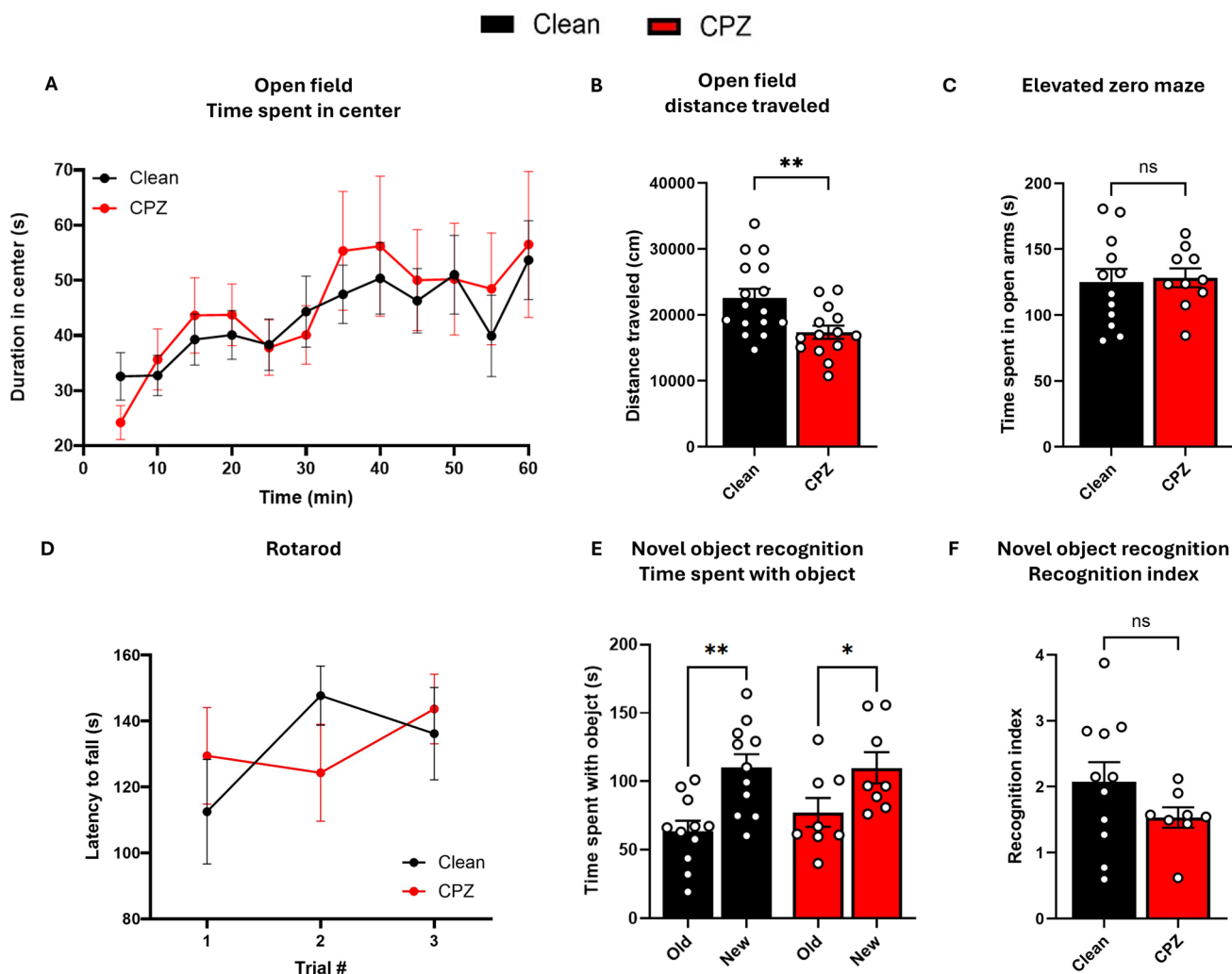


**Fig. 6** Behavioural outcomes of early age demyelination. **(A)** Time spent in the center of the open field arena was unchanged between groups (Clean,  $n=15$ ; CPZ,  $n=12$ ; two-way repeated measure ANOVA: time factor,  $P=0.0005$ ; group factor,  $P=0.7677$ , interaction,  $P=0.8179$ ). **(B)** CPZ exposure results in lower distance traveled over 60 min in the open field arena, compared to Clean group (Clean,  $n=16$ ; CPZ,  $n=14$ ; Student's  $t$ -test,  $P=0.006$ ). **(C)** Time spent in open arms of the EZM was unchanged between groups (Clean,  $n=12$ ; CPZ,  $n=10$ ; Student's  $t$ -test,  $P=0.735$ ). **(D)** Latency to fall in the rotarod test was unchanged

between groups across trials (Clean,  $n=16$ ; CPZ,  $n=14$ ; two-way ANOVA: time (trial) factor,  $P=0.2164$ ; group factor,  $P=0.9802$ , interaction,  $P=0.1859$ ). **E-F** No significant differences in performance were found between groups in the novel object recognition test **(E)** Time spent with each object in the testing phase (Clean,  $n=11$ ; CPZ,  $n=8$ ; two-way ANOVA, object type (within-subject),  $P=0.0009$ ,  $P=0.019$ ; group factor (between subject),  $P=0.5080$ ; interaction,  $P=0.4815$ ). **(F)** Recognition index (Clean,  $n=11$ ; CPZ,  $n=8$ ; Student's  $t$ -test,  $P=0.709$ ).

adult-onset demyelination, leaving the consequences of demyelination during earlier developmental stages less understood.

Demyelination, however, can occur at any age. POMS (Capasso et al., 2023) and traumatic brain injury in young individuals (Mahoney et al., 2022) provide notable examples. POMS cases are frequently associated with greater disability and brain atrophy, with more severe outcomes appearing earlier in life (McKay et al., 2019; Ruet, 2018). Furthermore, early asymptomatic lesions are often detected in AOMS patients long before diagnosis (Jakimovski et al., 2023; Patti et al., 2022; Van Der Valk & Amor, 2009),

raising critical questions about the consequences of early-onset demyelination.

Here, we evaluated whether the widely used CPZ model, typically applied to study adult demyelination, can also be used to investigate early-onset demyelination. We examined CPZ exposure in young mice compared with age-matched clean-diet controls, focusing on six ROIs to assess susceptibility to CPZ-induced damage and associated cellular and behavioral outcomes.

Although *Mbp* transcript levels were reduced in demyelinated regions, changes in OL populations were less pronounced than expected. This may reflect the high rate

of myelin turnover during the 4–8-weeks of age period in mice, which corresponds to adolescence in humans (de Faria et al., 2021). During this developmental stage, accelerated myelination occurs in regions involved in behavioral modulation and skill acquisition, including the myelination of previously unmyelinated axons that contribute to these processes (Rokach et al., 2024). Moreover, in a cohort of children with acquired white matter (WM) disorders, recurring WM lesions were associated with mild deficits in the first year and long-lasting effects over the subsequent 5–7 years (O'Mahony et al., 2015). This rapid myelin reorganization and seemingly effective regeneration may mask CPZ toxicity or reduce overall vulnerability. A longer or more intense exposure may therefore be required to reveal stronger effects in juvenile mice.

While *Iba1* transcript level increased in demyelinated regions, the density of *Iba1*-positive cells did not change, suggesting activation of resident microglia rather than a broad neuroinflammatory response involving recruitment of additional microglia to lesion sites (Lampron et al., 2015; Lloyd & Miron, 2019; Yang et al., 2012). Interestingly, early-life stress has been shown to leave a lasting imprint on maturing microglia and alter their responsiveness to stress later in life (Catale et al., 2020). A longer-term study of the consequences of early CPZ exposure, combined with a more detailed analysis of microglial activation, could help clarify the role of early-life neuroinflammation in the long-lasting deficits observed in POMS (McKay et al., 2019; Ruet, 2018).

Behaviorally, CPZ-exposed mice exhibited reduced locomotion, consistent with motor deficits reported in adult demyelination models (Franco-Pons et al., 2007; Sen et al., 2020). However, other behavioral outcomes were minimal, suggesting that early-onset demyelination may not produce the same breadth of clinical symptoms observed in adult models. While the reduced overall body weight of the CPZ-exposed mice is consistent with studies on adult animals (Kipp et al., 2009; Leopold et al., 2019), and could be a confound to the behavioral outcomes, the pronounced demyelination in the CTX likely contributed to locomotor deficits, resembling early clinical signs of disability in POMS.

Interestingly, the limited behavioral changes seen in our study may parallel the asymptomatic early lesions observed in AOMS patients. Thus, this early-exposure model may provide a useful approach for investigating WM lesions that precede clinical symptoms. Expanding behavioral testing beyond traditional MS-validated assays could also help identify early biomarkers or subclinical indicators of demyelination, opening opportunities for earlier diagnosis and intervention in MS and related demyelinating disorders.

## Materials and Methods

### Animals

C57Bl/6J male mice (Jackson Laboratory, stock no. 000664), regardless of their experimental group, were housed in groups of 2–5 per cage at a stable temperature of 24 °C, under a 12-h light–dark cycle (lights on at 7:00 AM, off at 7:00 PM), with unrestricted access to food and water. On postnatal day 12 (P12), mice were tattooed using a fine needle and biologically graded blue ink to mark a single digit on their hind paws. Only one digit was tattooed per animal.

All experimental procedures received approval from the Tel Aviv University Institutional Animal Care and Use Committee and the Israel Ministry of Health (TAU—LS—IL—2307—143—4).

### Cuprizone Exposure

At P30 mice were assigned to either Clean diet or CPZ-exposure groups, housed in cages containing 2–4 male littermates. Fresh rodent chow was ground using a high-speed food processor for 1 min. The chow was then weighed and either distributed as-is into petri dishes or mixed with CPZ powder (C9012, Merck) for a final concentration of 0.2%. Ground chow was freshly prepared every 48 h and placed in clean, flat petri dishes on the floor of each cage to allow easy access. The quantity of chow was monitored regularly to ensure ad libitum access.

Mice were maintained on either the clean or CPZ-supplemented chow for a duration of five weeks. Body weight was recorded once a week, and each mouse underwent visual assessments for fur condition, teeth length, and general health three times a week, following the food replacement. Wooden sticks were provided as environmental enrichment, allowing the mice to file their teeth and prevent overgrowth.

### Behavioral Assays

Behavioral tests were based on previously described assays (Levy, et al., 2025; Ophir et al., 2023). All tests were conducted during the light cycle (07:00–19:00). Mice were acclimatized to the testing room for at least 1 h before each session. The room temperature was maintained between 20 and 24 °C throughout all experiments, and lighting conditions were verified prior to each test. All mice participated in every test, with a minimum interval of 3 days between tests. The experimenter remained blind to the diet the mice were on.

## Open Field Test

Mice were placed in a Plexiglas box (40 cm × 40 cm × 30 cm) to assess spontaneous locomotor activity, which was recorded for 1 h. The area 10 cm from the walls was defined as the margin. Light intensity was set to ~60 lux in the center of the arena and ~10 lux at the margins. Mouse movements were tracked using Ethovision XT14 software.

## Rotarod Test

Mice were placed on a rotating rod (Catalog no. 47650, Ugo Basile), initially spinning at 4 rpm. After ensuring proper orientation on the rod, the rotation speed gradually increased to 40 rpm, with a 5-min time limit. To discourage mice from gripping the rod and hanging instead of walking, the rod diameter was increased to 30 cm using 3D-printed adapters. Mice that either gripped the rod for more than two full rotations or fell off within 20 s of the trial start were excluded from the analysis (Excluded Clean,  $n=2$ , CPZ,  $n=3$ ). Each mouse underwent three trials on the same day, with a 1 h rest period between trials.

## Elevated Zero Maze

Mice were placed in the closed arm of an elevated zero maze (60 cm high), and their movement was recorded for 5 min. The light intensity in the closed arms was set to ~10 lux and the open arms to ~60 lux. Ethovision XT14 software was used to track the mice's movements, and the time spent in the open arms was measured.

## Novel Object Recognition Test

Adapted from Leger et al. (2013), this test involved placing a mouse in a Plexiglas box (40 cm × 40 cm × 30 cm) with two identical objects. Spontaneous locomotion was recorded for 15 min. After a 4 h interval, one object was replaced with a novel one, and the test was repeated for another 15 min. Light intensity was set to ~40 lux across the arena, and mouse movements and interactions with the objects were tracked using Ethovision XT14 software.

The recognition index was calculated as the time spent exploring the novel object divided by the total exploration time for both objects.

## Brain Tissue Extraction

### Perfusions

Following behavioral experiments, mice were euthanized using an isoflurane chamber. Mice underwent transcardial

perfusion with 15 mL of ice-cold PBS solution and 15 mL of ice-cold solution of 4% paraformaldehyde, pH 7.4 (PFA, Sigma-Aldrich) diluted in PBS. Mice were decapitated and whole brain was carefully removed from the skull and placed in 4% PFA in 4 °C for 24 h to facilitate proper fixation. Brains were kept in PBS at 4 °C for up to two weeks before cellular and molecular assays were performed.

### Dissections

Mice were euthanized via cervical dislocation, followed by decapitation using sharp scissors to carefully extract the whole brain from the skull. The brains were immediately placed in a petri dish containing cold PBS for dissection. Using sterilized surgical instruments, the brains were coronally sectioned at 1 mm intervals, and each section was examined under a stereomicroscope (Olympus) for precise regional dissection. The following brain regions were isolated and transferred into separate sterile 2 mL tubes: mCC, motor cortex, striatum, hippocampus, amygdala and hypothalamus. To preserve sample integrity, the tubes were flash-frozen in liquid nitrogen and stored at -80 °C until molecular analyses were conducted. To ensure sterility and prevent contamination, all surgical tools and equipment were sterilized with ethanol and treated with RNase inhibitors (RNase-ExitusPlus, Biological Industries). All procedures were performed rapidly to minimize RNA and protein degradation.

## Cellular and Molecular Assays

### Immunofluorescence Staining

Fixed brains were coronally sectioned at a thickness of 50 μm using a vibratome (Leica). IF staining was done as previously described (Fischer, et al., 2022). Briefly, slices were washed three times with PBS for 5 min each, followed by permeabilization with 1.2% Triton X-100 in PBS for 15 min at room temperature (RT), and another three PBS washes (5 min each). Slices were then incubated in a blocking solution containing 5% normal goat serum (S1000, Vector Laboratories), 2% bovine serum albumin (A7030, Sigma-Aldrich), and 0.2% Triton X-100 in PBS for 1 h at RT. Primary antibodies, diluted in the blocking solution, were added to wells of a 96-well plate containing two brain slices per well, and incubated overnight at 4 °C. The following day, after three washes in PBS (15 min each), secondary antibodies conjugated to Alexa Fluor 488, 555, or 647 (1:1,000; ab150165—ABCAM, A32932, and A21247, Thermo Fisher Scientific) were added in blocking solution for 1 h at RT. The slices were then washed three times in PBS for 15 min each and mounted onto pre-coated glass

**Table 2** qPCR primers used in this study

Origin	Forward	Reverse
<i>Gapdh</i>	5' GCCTCCGTGTTCTACC 3'	5' CCTCAGTGTAGCCCAAGATG 3'
<i>Mbp</i>	5' CCTCAGTGTAGCCCAAGATG 3'	5' CCTCAGTGTAGCCCAAGATG 3'
<i>Iba1</i>	5' TCTGCCGTCCAAACTTGAAG 3'	5' GTTCTCCAGCATTTCGCTTC 3'

slides (Bar-Naor) using VECTASHIELD Hardset Antifade Mounting Medium with DAPI (Vector Laboratories).

The primary antibodies used were anti-ASPA (1:100; sc-377308, Santa Cruz), anti-PDGFR $\alpha$  (CD140a, 14–1401-82, Invitrogen), anti-MBP (1:500, MAB386, Sigma-Aldrich), and anti-Iba1 (1:500, 234,006, SYSY). For ASPA staining, an antigen retrieval step was included prior to permeabilization. Slices were incubated at 70 °C in sodium citrate buffer (pH 8.5) for 30 min, then cooled to RT for 10 min. Slices were washed twice in PBS for 15 min each, and the staining protocol was resumed as described.

### Quantification of Cellular Properties

Fluorescence images were acquired using a light microscope (Olympus IX83) at either 10 $\times$  or 20 $\times$  magnification, depending on the specific staining and analysis requirements. Image analysis was conducted using Fiji-ImageJ software. Both imaging and analysis were performed by an experimenter blinded to treatment conditions. Cell counts, including microglia, OPCs, and mOLs, were manually quantified using the multipoint tool. Mbp intensity was assessed by calculating the sum of positive pixels within the image. Gross anatomical features were measured using the freehand lasso tool in Fiji-ImageJ.

### RNA Extraction and cDNA Preparation

RNA extraction was performed as previously described (Bar et al., 2024), with minor changes. Stainless steel beads were placed in 2 mL tubes containing regional brain tissue along with 500  $\mu$ L of cold TRIzol reagent (Thermo Fisher Scientific). Tissue homogenization was carried out using a TissueLyser 2 (Qiagen) for 60 s at a frequency of 24,000 Hz. Once homogenization was complete, an additional 500  $\mu$ L of TRIzol was added, and the samples were incubated at RT for 5 min. Next, 200  $\mu$ L of chloroform (Bio-Lab) were added to each sample, followed by manual shaking for 15 s and a further 3 min incubation at RT. Samples were centrifuged for 20 min at 4 °C at 13,800 rpm (800 $\times$ g) using an Eppendorf 5430R centrifuge. This process separated the homogenate into protein, DNA, and RNA phases, with the RNA layer positioned on top. The RNA layer was carefully transferred to new tubes and mixed with an equal volume of isopropanol (Bio-Lab). After manual shaking and 5 min of RT incubation, the samples were centrifuged for 15 min

at 4 °C and 13,800 rpm (800 $\times$ g), which precipitated the RNA. The isopropanol was then discarded, and the RNA pellet was washed twice with 1 mL of cold 80% ethanol (Sigma-Aldrich) diluted in DEPC-treated water (Biological Industries), followed by 5 min centrifugation for each wash. Following ethanol removal, the tubes were left open for approximately 90 min to allow the remaining ethanol to evaporate. The RNA was resuspended in 12  $\mu$ L of DEPC-treated water and heated at 60 °C for 3 min. Samples were pipetted thoroughly to ensure even concentration, and RNA quantity and purity were measured using a NanoDrop One device (Thermo Fisher Scientific). The extracted RNA was stored at -80 °C.

For reverse transcription, RNA samples were diluted to a concentration of 0.4–10 ng/ $\mu$ L. cDNA synthesis was performed using random primers and the High-Capacity cDNA Reverse Transcription Kit (Thermo Fisher Scientific) according to the following protocol in a C1000 Touch thermal cycler: 10 min at 25 °C, 120 min at 37 °C, 5 min at 85 °C, and a final hold at 4 °C. The resulting cDNA was stored at -20 °C for future use.

### Quantitative PCR (qPCR)

mRNA expression levels were quantified using qPCR with the Fast SYBR Green PCR Master Mix (Thermo Fisher Scientific) and the Bio-Rad CFX Connect quantitative PCR Detection System. The qPCR protocol began with an initial denaturation at 95 °C for 20 s, followed by 40 amplification cycles. Each cycle consisted of denaturation at 95 °C for 3 s and annealing/extension at 60 °C for 30 s. A melt curve analysis was also performed by holding the samples at 60 °C for 5 s, then increasing the temperature by 0.5 °C increments every 5 s until reaching 95 °C.

mRNA levels were determined using the comparative cycle threshold (Ct) method (Schmittgen & Livak, 2008). Target gene expression was normalized to glyceraldehyde 3-phosphate dehydrogenase (*Gapdh*) as a reference gene, and the results are presented as fold change relative to the control group. All primers were purchased from Hy-Laboratories and diluted to a concentration of 10 mM following the manufacturer's instructions, using DEPC-treated water. Primer sequences are provided in Table 2.

## Statistical Analysis

All data collection was conducted by an experimenter blinded to the experimental groups. The normality of datasets was assessed using D'Agostino-Pearson or Shapiro–Wilk tests. For datasets with normal distributions, statistical analysis was performed using unpaired two-tailed Student's t-tests (Prism, GraphPad Software). Non-normally distributed data were analysed using the Wilcoxon signed-rank test. Results are expressed as mean±standard error of the mean (SEM), and statistical significance was set at  $p < 0.05$  (\*  $p < 0.05$ , \*\*  $p < 0.01$ , \*\*\*  $p < 0.001$ , \*\*\*\*  $p < 0.0001$ ). Outliers were identified using the Grubbs' test at a significance level of  $p < 0.05$ .

**Supplementary Information** The online version contains supplementary material available at <https://doi.org/10.1007/s12017-026-08911-2>.

**Author Contributions** R.M and L.G performed the experiments. R.M, G.ES and B.B designed and managed the experiments. R.M and B.B wrote the manuscript.

**Funding** Open access funding provided by Tel Aviv University.

**Data Availability** All data supporting the findings of this study are available within the paper.

## Declarations

**Competing Interests** The authors declare no competing interests.

**Open Access** This article is licensed under a Creative Commons Attribution 4.0 International License, which permits use, sharing, adaptation, distribution and reproduction in any medium or format, as long as you give appropriate credit to the original author(s) and the source, provide a link to the Creative Commons licence, and indicate if changes were made. The images or other third party material in this article are included in the article's Creative Commons licence, unless indicated otherwise in a credit line to the material. If material is not included in the article's Creative Commons licence and your intended use is not permitted by statutory regulation or exceeds the permitted use, you will need to obtain permission directly from the copyright holder. To view a copy of this licence, visit <http://creativecommons.org/licenses/by/4.0/>.

## References

- Anagnostouli, M., Markoglou, N., & Chrousos, G. (2020). Psycho-neuro-endocrino-immunologic issues in multiple sclerosis: A critical review of clinical and therapeutic implications. *Hormones (Athens, Greece)*, *19*, 485–496.
- Ascherio, A. (2013). Environmental factors in multiple sclerosis. *Expert Review of Neurotherapeutics*, *13*, 3–9.
- Averbeck, B. B., & Murray, E. A. (2020). Hypothalamic interactions with large-scale neural circuits underlying reinforcement learning and motivated behavior. *Trends in Neurosciences*, *43*, 681–694.
- Bar, E., & Barak, B. (2019). Microglia roles in synaptic plasticity and myelination in homeostatic conditions and neurodevelopmental disorders. *Glia*, *67*, 2125–2141.
- Bar, E., et al. (2024). Neuronal deletion of Gtf2i results in developmental microglial alterations in a mouse model related to Williams syndrome. *Glia*, *72*, 1117–1135.
- Bermel, R. A., & Bakshi, R. (2006). The measurement and clinical relevance of brain atrophy in multiple sclerosis. *Lancet Neurology*, *5*, 158–170.
- Bénardais, K., et al. (2013). Cuprizone [bis(cyclohexylidenehydrazide)] is selectively toxic for mature oligodendrocytes. *Neurotoxicity Research*, *24*, 244–250.
- Bradl, M., & Lassmann, H. (2010). Oligodendrocytes: Biology and pathology. *Acta Neuropathologica*, *119*, 37–53.
- Burdakov, D., & Peleg-Raibstein, D. (2020). The hypothalamus as a primary coordinator of memory updating. *Physiology & Behavior*, *223*, Article 112988.
- Calabrese, M., et al. (2010). Imaging distribution and frequency of cortical lesions in patients with multiple sclerosis. *Neurology*, *75*, 1234–1240.
- Capasso, N., et al. (2023). Aging in multiple sclerosis: From childhood to old age, etiopathogenesis, and unmet needs: A narrative review. *Frontiers in Neurology*, *14*, Article 1207617.
- Caria, A. A. (2023). A hypothalamic perspective of human socioemotional behavior. *The Neuroscientist*. <https://doi.org/10.1177/10738584221149647>
- Catale, C., Gironde, S., Iacono, L. L., & Carola, V. (2020). Microglial function in the effects of early-life stress on brain and behavioral development. *Journal of Clinical Medicine*, *9*, 468.
- Cavallari, M., et al. (2014). Microstructural changes in the striatum and their impact on motor and neuropsychological performance in patients with multiple sclerosis. *PLoS ONE*, *9*, Article e101199.
- Chang, A., Nishiyama, A., Peterson, J., Prineas, J., & Trapp, B. D. (2000). NG2-positive oligodendrocyte progenitor cells in adult human brain and multiple sclerosis lesions. *Journal of Neuroscience*, *20*, 6404–6412.
- de Faria, O., et al. (2021). Periods of synchronized myelin changes shape brain function and plasticity. *Nature Neuroscience*, *24*(11), 1508–1521.
- Degraeve, B., Sequeira, H., Mecheri, H., & Lenne, B. (2022). Corpus callosum damage to account for cognitive, affective, and social-cognitive dysfunctions in multiple sclerosis: A model of callosal disconnection syndrome? *Multiple Sclerosis Journal*, *29*, 160–168. <https://doi.org/10.1177/13524585221091067>
- Dighriri, I. M., et al. (2023). An overview of the history, pathophysiology, and pharmacological interventions of multiple sclerosis. *Cureus*, *15*, Article e33242.
- Dobson, R., & Giovannoni, G. (2019). Multiple sclerosis—A review. *European Journal of Neurology*, *26*, 27–40.
- Domingues, H. S., Portugal, C. C., Socolato, R., & Relvas, J. B. (2016). Oligodendrocyte, astrocyte, and microglia crosstalk in myelin development, damage, and repair. *Frontiers in Cell and Developmental Biology*, *4*, Article 202589.
- Dorikhani, A., Omid, A., Movahedin, M., & Halvaei, I. (2024). Chronic demyelination interferes with normal spermatogenesis in cuprizone-intoxicant C57/BL 6 mice: An experimental study. *International Journal of Reproductive BioMedicine*, *22*, 43–54.
- Eden, D., et al. (2019). Spatial distribution of multiple sclerosis lesions in the cervical spinal cord. *Brain*, *142*, 633–646.
- Erö, C., Gewaltig, M. O., Keller, D., & Markram, H. (2018). A cell atlas for the mouse brain. *Frontiers in Neuroinformatics*, *12*, Article 421921.
- Filippi, M., et al. (2019). Assessment of lesions on magnetic resonance imaging in multiple sclerosis: Practical guidelines. *Brain*, *142*, 1858–1875.

- Fischer, I., et al. (2022). Hyperbaric oxygen therapy alleviates social behavior dysfunction and neuroinflammation in a mouse model for autism spectrum disorders. *International Journal of Molecular Sciences*, 23, 11077.
- Fisher, K. S., Cuascut, F. X., Rivera, V. M., & Hutton, G. J. (2020). Current advances in pediatric onset multiple sclerosis. *Biomedicine*, 8, Article 71.
- Flurkey, K., Curren, J. M., & Harrison, D. E. (2007). Mouse models in aging research. *The Mouse in Biomedical Research*, 3, 637–672.
- Franco-Pons, N., Torrente, M., Colomina, M. T., & Vilella, E. (2007). Behavioral deficits in the cuprizone-induced murine model of demyelination/remyelination. *Toxicology Letters*, 169, 205–213.
- Frankenhaeuser, B. (1952). The hypothesis of saltatory conduction. *Cold Spring Harbor Symposia on Quantitative Biology*, 17, 27–36.
- Franklin, R. J. M. (2002). Why does remyelination fail in multiple sclerosis? *Nature Reviews Neuroscience*, 3(9), 705–714. <https://doi.org/10.1038/nrn917>
- Franklin, R. J. M., & Ffrench-Constant, C. (2008). Remyelination in the CNS: From biology to therapy. *Nature Reviews Neuroscience*, 9(11), 839–855.
- Franklin, R. J. M., & Kotter, M. R. (2008). The biology of CNS remyelination: The key to therapeutic advances. *Journal of Neurology*, 255, 19–25.
- Genç, B., Şen, S., Aslan, K., & İncesu, L. (2023). Volumetric changes in hypothalamic subunits in patients with relapsing remitting multiple sclerosis. *Neuroradiology*, 65, 899–905.
- Goldberg, J., Clarner, T., Beyer, C., & Kipp, M. (2015). Anatomical distribution of cuprizone-induced lesions in C57BL/6 mice. *Journal of Molecular Neuroscience*, 57, 166–175.
- Hamilton, S. P., & Rome, L. H. (1994). Stimulation of in vitro myelin synthesis by microglia. *Glia*, 11, 326–335.
- Hochstrasser, T., Exner, G. L., Nyamoya, S., Schmitz, C., & Kipp, M. (2017). Cuprizone-containing pellets are less potent to induce consistent demyelination in the corpus callosum of C57BL/6 mice. *Journal of Molecular Neuroscience*, 61, 617–624.
- Hoffmann, K., Lindner, M., Gröticke, I., Stangel, M., & Löscher, W. (2008). Epileptic seizures and hippocampal damage after cuprizone-induced demyelination in C57BL/6 mice. *Experimental Neurology*, 210, 308–321.
- Ito, D., et al. (1998). Microglia-specific localisation of a novel calcium binding protein, Iba1. *Brain Research. Molecular Brain Research*, 57, 1–9.
- Jakimovski, D., et al. (2023). Improvement in time to multiple sclerosis diagnosis: 25-year retrospective analysis from New York State MS Consortium (NYSMSC). *Multiple Sclerosis Journal*, 29, 753–756.
- Kerbrat, A., et al. (2020). Multiple sclerosis lesions in motor tracts from brain to cervical cord: Spatial distribution and correlation with disability. *Brain*, 143, 2089–2105.
- Kinches, Z. T., et al. (2011). Lesion probability mapping to explain clinical deficits and cognitive performance in multiple sclerosis. *Multiple Sclerosis Journal*, 17, 681–689.
- Kipp, M., Clarner, T., Dang, J., Copray, S., & Beyer, C. (2009). The cuprizone animal model: New insights into an old story. *Acta Neuropathologica*, 118, 723–736.
- Kopanitsa, M. V., et al. (2021). Cognitive disturbances in the cuprizone model of multiple sclerosis. *Genes, Brain, and Behavior*, 20, Article e12663.
- Kurtzke Expanded Disability Status Scale - Multiple Sclerosis Centers of Excellence. (2021). [https://www.va.gov/MS/Professionals/diagnosis/Kurtzke\\_Expanded\\_Disability\\_Status\\_Scale.asp](https://www.va.gov/MS/Professionals/diagnosis/Kurtzke_Expanded_Disability_Status_Scale.asp)
- Lampron, A., et al. (2015). Inefficient clearance of myelin debris by microglia impairs remyelinating processes. *Journal of Experimental Medicine*, 212, 481–495.
- Leger, M., et al. (2013). Object recognition test in mice. *Nature Protocols*, 8(12), 2531–2537.
- Leopold, P., Schmitz, C., & Kipp, M. (2019). Animal weight is an important variable for reliable cuprizone-induced demyelination. *Journal of Molecular Neuroscience*, 68(4), 522–528.
- Levy, G., et al. (2025). Gtf2i-encoded transcription factor Tfii-i regulates myelination via Sox10 and Mbp regulatory elements. *Nature Communications*, 16(1), 1–24.
- Lloyd, A. F., & Miron, V. E. (2019). The pro-remyelination properties of microglia in the central nervous system. *Nature Reviews Neurology*, 15(8), 447–458.
- Lubetzki, C., Zalc, B., Williams, A., Stadelmann, C., & Stankoff, B. (2020). Remyelination in multiple sclerosis: From basic science to clinical translation. *Lancet Neurology*, 19, 678–688.
- Lubrich, C., Giesler, P., & Kipp, M. (2022). Motor behavioral deficits in the cuprizone model: Validity of the rotarod test paradigm. *International Journal of Molecular Sciences*, 23, 11342.
- Luo, C., et al. (2017). The role of microglia in multiple sclerosis. *Neuropsychiatric Disease and Treatment*, 13, 1661–1667.
- Mahoney, S. O., Chowdhury, N. F., Ngo, V., Imms, P., & Irimia, A. (2022). Mild traumatic brain injury results in significant and lasting cortical demyelination. *Frontiers in Neurology*, 13, Article 854396.
- Marques, S., Zeisel, A., Codeluppi, S., Van Bruggen, D., Falcão, A. M., Xiao, L., Li, H., Häring, M., Hochgerner, H., Romanov, R. A., Gyllborg, D., Muñoz-Manchado, A. B., LaManno, G., Lönnnerberg, P., Floriddia, E. M., Rezayee, F., Ernfors, P., Arenas, E., Hjerling-Leffler, J., ... Castelo-Branco, G. (2016). Oligodendrocyte heterogeneity in the mouse juvenile and adult central nervous system. *Science (New York, N.Y.)*, 352(6291), 1326–1329. <https://doi.org/10.1126/science.aaf6463>
- Matsushima, G. K., & Morell, P. (2001). The neurotoxicant, cuprizone, as a model to study demyelination and remyelination in the Central Nervous System. *Brain Pathology*, 11, 107–116.
- McKay, K. A., Hillert, J., & Manouchehrinia, A. (2019). Long-term disability progression of pediatric-onset multiple sclerosis. *Neurology*, 92, E2764–E2773.
- Millward, J. M., et al. (2020). Transient enlargement of brain ventricles during relapsing-remitting multiple sclerosis and experimental autoimmune encephalomyelitis. *JCI Insight*. <https://doi.org/10.1172/jci.insight.140040>
- Murúa, S. R., Farez, M. F., & Quintana, F. J. (2021). The immune response in multiple sclerosis. *Annual Review of Pathology, Mechanisms of Disease*, 17, 121–139.
- Nave, K. A., & Werner, H. B. (2014). Myelination of the nervous system: Mechanisms and functions. *Annual Review of Cell and Developmental Biology*, 30, 503–533.
- Noori, R., et al. (2020). Activity-dependent myelination: A glial mechanism of oscillatory self-organization in large-scale brain networks. *Proceedings of the National Academy of Sciences*, 117, 13227–13237.
- O'Mahony, J., et al. (2015). Recovery from central nervous system acute demyelination in children. *Pediatrics*, 136, e115–e123.
- Ophir, O., et al. (2023). Deletion of Gtf2i via systemic administration of AAV-PHP.eB virus increases social behavior in a mouse model of a neurodevelopmental disorder. *Biomedicine*, 11, 2273.
- Patsopoulos, N. A. (2018). Genetics of multiple sclerosis: An overview and new directions. *Cold Spring Harbor Perspectives in Medicine*. <https://doi.org/10.1101/cshperspect.a028951>
- Patti, F., et al. (2022). Factors driving delayed time to multiple sclerosis diagnosis: Results from a population-based study. *Multiple Sclerosis and Related Disorders*. <https://doi.org/10.1016/j.msard.2021.103361>
- Peres, D. S., et al. (2022). Prevalence of depression and anxiety in the different clinical forms of multiple sclerosis and associations with

- disability: A systematic review and meta-analysis. *Brain, Behavior, & Immunity*, 24, Article 100484.
- Pfeifenbring, S., Nessler, S., Wegner, C., Stadelmann, C., & Brück, W. (2015). Remyelination after cuprizone-induced demyelination is accelerated in juvenile mice. *Journal of Neuropathology and Experimental Neurology*, 74, 756–766.
- Ponath, G., Park, C., & Pitt, D. (2018). The role of astrocytes in multiple sclerosis. *Frontiers in Immunology*, 9, Article 337102.
- Pott, F., et al. (2009). Cuprizone effect on myelination, astrogliosis and microglia attraction in the mouse basal ganglia. *Brain Research*, 1305, 137–149.
- Praet, J., Guglielmetti, C., Berneman, Z., Van der Linden, A., & Ponsaerts, P. (2014). Cellular and molecular neuropathology of the cuprizone mouse model: Clinical relevance for multiple sclerosis. *Neuroscience and Biobehavioral Reviews*, 47, 485–505.
- Rocca, M. A., et al. (2018). The hippocampus in multiple sclerosis. *Lancet Neurology*, 17, 918–926.
- Rokach, M., et al. (2024). Tackling myelin deficits in neurodevelopmental disorders using drug delivery systems. *Advanced Drug Delivery Reviews*, 207, Article 115218.
- Ruet, A. (2018). Update on pediatric-onset multiple sclerosis. *Revue Neurologique (Paris)*, 174, 398–407.
- Saab, A. S., Tzvetanova, I. D., & Nave, K. A. (2013). The role of myelin and oligodendrocytes in axonal energy metabolism. *Current Opinion in Neurobiology*, 23, 1065–1072.
- Santos, E. N., & Douglas Fields, R. (2021). Regulation of myelination by microglia. *Science Advances*, 7, Article 1131.
- Schmittgen, T. D., & Livak, K. J. (2008). Analyzing real-time PCR data by the comparative CT method. *Nature Protocols*, 3, 1101–1108.
- Seidl, A. H. (2014). Regulation of conduction time along axons. *Neuroscience*, 276, 126–134.
- Sen, M. K., Almuslehi, M. S. M., Coorsen, J. R., Mahns, D. A., & Shortland, P. J. (2020). Behavioural and histological changes in cuprizone-fed mice. *Brain, Behavior, and Immunity*, 87, 508–523.
- Sen, M. K., Mahns, D. A., Coorsen, J. R., & Shortland, P. J. (2019). Behavioural phenotypes in the cuprizone model of central nervous system demyelination. *Neuroscience and Biobehavioral Reviews*, 107, 23–46.
- Siva, A. (2013). Asymptomatic MS. *Clinical Neurology and Neurosurgery*, 115, S1–S5.
- Skripuletz, T., et al. (2013). Astrocytes regulate myelin clearance through recruitment of microglia during cuprizone-induced demyelination. *Brain*, 136, 147–167.
- Tepavčević, V., & Lubetzki, C. (2022). Oligodendrocyte progenitor cell recruitment and remyelination in multiple sclerosis: The more, the merrier? *Brain*, 145, 4178–4192.
- Tonietto, M., et al. (2023). Periventricular remyelination failure in multiple sclerosis: A substrate for neurodegeneration. *Brain*, 146, 182–194.
- Torkildsen, O., Brunborg, L. A., Myhr, K. M., & Bø, L. (2008). The cuprizone model for demyelination. *Acta Neurologica Scandinavica*, 117, 72–76.
- Touma, L., & Muccilli, A. (2022). Diagnosis and management of Central Nervous System demyelinating disorders. *Neurologic Clinics*, 40, 113–131.
- Valério-Gomes, B., Guimarães, D. M., Szczupak, D., & Lent, R. (2018). The absolute number of oligodendrocytes in the adult mouse brain. *Frontiers in Neuroanatomy*, 12, Article 398556.
- Van Der Valk, P., & Amor, S. (2009). Preactive lesions in multiple sclerosis. *Current Opinion in Neurology*, 22, 207–213.
- van Munster, C. E. P., Jonkman, L. E., Weinstein, H. C., Uitdehaag, B. M., & Geurts, J. J. (2015). Gray matter damage in multiple sclerosis: Impact on clinical symptoms. *Neuroscience*, 303, 446–461.
- Vega-Riquer, J. M., Mendez-Victoriano, G., Morales-Luckie, R. A., & Gonzalez-Perez, O. (2019). Five decades of cuprizone, an updated model to replicate demyelinating diseases. *Current Neuropharmacology*, 17, 129–141.
- Voet, S., Prinz, M., & van Loo, G. (2019). Microglia in central nervous system inflammation and multiple sclerosis pathology. *Trends in Molecular Medicine*, 25, 112–123.
- Walton, C., et al. (2020). Rising prevalence of multiple sclerosis worldwide: Insights from the Atlas of MS, third edition. *Multiple Sclerosis (Houndmills, Basingstoke, England)*, 26, 1816.
- Wang, H., et al. (2013). Cuprizone-induced demyelination in mice: Age-related vulnerability and exploratory behavior deficit. *Neuroscience Bulletin*, 29, 251–259.
- Xin, W., & Chan, J. R. (2020). Myelin plasticity: Sculpting circuits in learning and memory. *Nature Reviews Neuroscience*, 21(12), 682–694.
- Yang, T. T., et al. (2012). Differential distribution and activation of microglia in the brain of male C57BL/6J mice. *Brain Structure and Function*, 218(4), 1051–1060.
- Younger, D. S. (2023). Multiple sclerosis: Motor dysfunction. *Handbook of Clinical Neurology*, 196, 119–147.
- Zendedel, A., Beyer, C., & Kipp, M. (2013). Cuprizone-induced demyelination as a tool to study remyelination and axonal protection. *Journal of Molecular Neuroscience*, 51, 567–572.
- Zhan, J., et al. (2020). The cuprizone model: Dos and do not. *Cells*, 9(4), Article 843.
- Zheng, K., et al. (2018). Molecular and Genetic Evidence for the PDGFR $\alpha$ -Independent Population of Oligodendrocyte Progenitor Cells in the Developing Mouse Brain. *Journal of Neuroscience*, 38, 9505–9513.
- Zirngibl, M., Assinck, P., Sizov, A., Caprariello, A. V., & Plemel, J. R. (2022). Oligodendrocyte death and myelin loss in the cuprizone model: An updated overview of the intrinsic and extrinsic causes of cuprizone demyelination. *Molecular Neurodegeneration*, 17, 34. <https://doi.org/10.1186/s13024-022-00538-8>

**Publisher's Note** Springer Nature remains neutral with regard to jurisdictional claims in published maps and institutional affiliations.